Antibacterial Inorganic Coating of Calcium Silicate Hydrate Substrates by Copper Incorporation

Thomas Schwartz,[§] Nils Schewe,[§] Matthias Schwotzer, Marita Heinle, Ammar Mahmood, Peter Krolla, and Peter Thissen*

ABSTRACT: Under environmental conditions, biofilms can oftentimes be found on different surfaces, accompanied by the structural degradation of the substrate. Since high-copper-content paints were banned in the EU, a solution for the protection of these surfaces has to be found. In addition to hydrophobation, making the surfaces inherently biofilm-repellent is a valid strategy. We want to accomplish this via the metal exchange in calcium silicate hydrate (CSH) substrates with transition metals. As has been shown with Europium, even small amounts of metal can have a great influence on the material properties. To effectively model CSH surfaces, ultrathin CSH films were grown on silicon wafers using $Ca(OH)_2$ solutions. Subsequently, copper was incorporated as an active component via ion exchange. Biofilm development is quantified using a multiple-resistant *Pseudomonas aeruginosa* strain described as a strong biofilm former cultivated in the culture medium for 24 h. Comprehensive structural and chemical analyses of the substrates are done by environmental scanning electron microscopy (ESEM), transmission Fourier transform infrared spectroscopy (FT-IR), X-ray photoelectron spectroscopy (XPS), and time-of-flight secondary ion mass spectrometry (ToF-SIMS). Results do not show any structural deformation of the substrates by the incorporation of the Cu combined with three-dimensional (3D) homogeneous distribution. While the copper-free CSH phase shows a completely random distribution of the bacteria in biofilms, the samples with copper incorporation reveal lower bacterial colonization of the modified surfaces with an enhanced cluster formation.

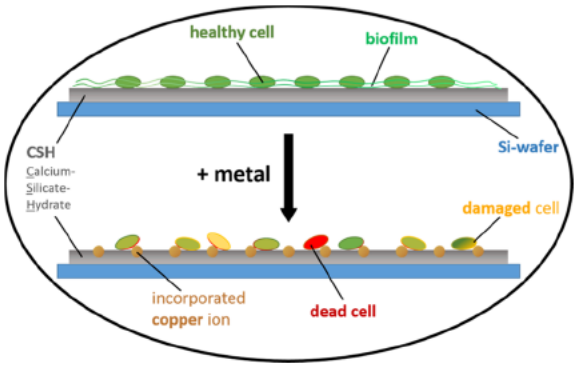

KEYWORDS: *coating, copper, calcium silicate hydrate, antibacterial, inorganic, cement*

INTRODUCTION

Today, organic coatings are a business of billions of dollars per years. Due to the high diversity in organic chemistry, tailored coatings exist for nearly every situation.[1,2] An actual bottleneck in surface science are so-called antibacterial coatings.[3−10]

Biofilms in technical facilities increase friction, energy needs, and pipe pressure drops, as well as decrease heat-transfer efficiency. Biofilms can also harbor dangerous pathogenic microorganisms, e.g., in potable water supplies. The genesis of biofouling formation occurs when microorganisms make a transition from the free-floating planktonic to a stationary sessile lifestyle, thus forming a biofilm.[11,12] They adhere to one another and hard surfaces with an adhesive called extracellular polymeric substance (EPS). The general principles of biofilm formation and factors leading to the settlement on hard surfaces are similar in medical, marine, and industrial applications.[13−16] Numerous substances are known to exhibit bactericidal properties, including numerous metals such as silver, zinc, and copper.[17] Bactericidal activities of metals are rarely specific to prokaryotic cells and are related to a certain degree of cytotoxicity, which can affect evolutionary higher organisms coming in contact with elevated concentrations of, e.g., copper. Hence, it is important that metals are immobilized in surface coating without any leaching effects.[11]

Today, Portland cement concrete is the world's most extensively used manufactured material.[18] The primary hydration product and the binding phase of Portland cement paste are calcium silicate hydrates (CSHs). The microorganism activities may be responsible for microstructural, mineralogical, and biochemical damages to these materials.[19] Protective coatings are reached, for instance, by the functionalization of CSH surfaces with water-repellent organic films.[20] Unfortunately, these organic films are weak against temperature and especially susceptible to abrasion. In 2019, we have shown that it is possible to prepare an intrinsically hydrophobic surface of

CSH phases just at room temperature.[21] Such a material is extremely robust to a harsh environment and could prolong the service lifetime of coated materials. CSH phases were grown on silicon wafers and brought into contact with Eu(III) solutions at room temperature. The exchange of the ions leads to several changes in the surface properties of the CSH material.[22] Doping of oxides with rare-earth oxides (REOs) can strongly influence their properties.

To effectively model CSH surfaces, we grow films of CSH on silicon wafers using $Ca(OH)_2$ solutions. We incorporate copper as an active component after the synthesis via ion exchange. Using model substrates ensures reproducibility and makes a variety of scientific analysis methods available. We focus on the chemical analysis of the surfaces, using environmental scanning electron microscopy (ESEM), transmission Fourier transform infrared spectroscopy (FT-IR), X-ray photoelectron spectroscopy (XPS), and time-of-flight secondary ion mass spectrometry (ToF-SIMS). Biofilms are applied from dispersions of different bacteria (modified *Pseudomonas aeruginosa*) in a culture medium and grown over 24 h. Antibacterial properties of the CSH and Cu-impregnated CSH coatings were investigated by fluorescence microscopy.

METHODOLOGY

Preparation of Samples. The 30 mm × 10 mm × 0.5 mm double-polished Si(111) wafers were coated with an approximately 180 nm thick calcium silicate hydrate (CSH) film using a 0.010 M $Ca(OH)_2$ solution. For this purpose, the wafers were first rinsed under flowing water, then treated in a 1:1 mixture of ethanol and water for 30 min in an ultrasonic bath, then rinsed again under flowing water, and finally submerged in a 1:3 (vol) mixture of H_2O_2 (30% wt aq., Sigma) and H_2SO_4 (98% wt aq., Sigma) for 45 min at 80 °C. The wafers were then placed in a freshly prepared 0.010 M $Ca(OH)_2$ solution for 48 h, rinsed with 2 mL water, and dried first under nitrogen and then in a vacuum. After drying, the wafers were impregnated with copper by submerging in a solution of $[Cu(NH_3)_4](OH)_2$ (0.001 M, NH_3 12.5% wt aq.) for 24 h. The wafers were again rinsed with 2 mL of water per side, dried in a vacuum, and stored under an N_2 protective atmosphere.

Characterization of Samples. *Environmental Scanning Electron Microscope (ESEM).* SEM images were acquired using a Philips XL 30 field emission gun environmental scanning electron microscope (FEG-ESEM) operated at an accelerating voltage of 20 kV in the high-vacuum mode.

Fourier Transform Infrared (FT-IR) Spectroscopy. FT-IR measurements were performed in an N_2-purged glovebox with a Bruker Vertex 70 and recorded with a nominal 4 cm^{-1} resolution. The spectra were collected from 400 to 4000 cm^{-1} in the transmission mode with an angle of incidence of 64° relative to the silicon surface normal. Per sample, 25 × 128 scans were recorded. A room-temperature pyroelectric detector (DTGS) was employed for data collection.

X-ray Photoelectron Spectroscopy (XPS). XP spectra were collected with a Quantum 2000 Scanning ESCA Microprobe (Physical Electronics) spectrometer equipped with a concentric hemispherical analyzer under ultrahigh-vacuum conditions with a base pressure below 1×10^{-9} mbar using an Al Kα (1486.6 eV) X-ray source. The spectra were recorded at a 90° take-off angle with respect to the surface. Analysis was performed with a pass energy of 200 eV for the survey and 50 eV for the core-level spectra. The latter were recorded for C 1s, O 1s, Ca 2p, Si 2p, and Cu 2p. The spectra obtained were analyzed using the CASA XPS software, and the surface sensitivity factors used to determine the atomic concentrations were taken from the MultiPak Version 6.0 software (supplied by Physical Electronics). The Ca $2p_{3/2}$ line was used for referencing the binding energies. All spectra were fitted with a Gauss−Lorentz profile (30% of Lorentz contribution) using a Shirley background. The spectral line positions were energy-calibrated for Ca $2p_{3/2}$ to be positioned at 346.6 eV.

Time-of-Flight Secondary Ion Mass Spectrometry (ToF-SIMS). The ToF-SIMS analysis was carried out on a gridles reflectron-based ToF-SIMS V instrument (ION-TOF GmbH, Muenster, Germany), equipped with a bismuth-cluster ion source. All spectra and images were obtained using Bi_3^+ primary ions at 25 keV energy in the high-current bunched mode, with a mass resolution of $m/\Delta m = 6000$ and a repetition rate of 10 kHz. The beam diameter was about 3−5 μm. For depth profiling, a 1 keV oxygen beam was applied. This sputter beam (232 nA) was scanned over an area of 500 × 500 μm^2, while data was recorded from a concentric 250 × 250 μm^2 field of view scanned with the Bi beam (0.34 pA target current). Mass scales were calibrated on small hydrocarbon fragments detected on every sample and ^{44}Ca.

Inductively Coupled Plasma-Optical Emission Spectroscopy (ICP-OES). For the leaching experiments, the wafers were stored in 10 mL of water for different times at room temperature to determine the degree of leaching. One treated wafer was then placed in the HCl solution (50% wt aq.) for 24 h to etch the entire coating. Aliquots from the different samples were finally analyzed by ICP-OES.

Living/Dead Discrimination. The *P. aeruginosa* strain PA49, which shows a strong biofilm-forming capacity, was used as a reference strain.

Biofilms colonizing the CSH and Cu−CSH coatings were characterized by (I) a living/dead discrimination and (II) the coverage rate of the attached bacterial cells using the Live/Dead BacLight Bacterial Viability Kit (ThermoFischer Scientific). The principle of this test system is two different DNA dyes intercalating with intracellular DNA, which can be detected by fluorescence microscopy analysis. The DNA of living bacterial cells can be specifically stained with Syto 9, which can be visualized as green fluorescence, whereas the DNA of dead or injured bacterial cells can be detected as a red fluorescent signal by the propidium iodide dye. The total coverage rate is calculated by the sum of both green and red fluorescent intensities according to the whole image size using the interactive area determination tool of the Zeiss ZEN blue analysis software.

Test Setup. Overnight cultures of Luria-Broth (LB media, 37 °C)-grown PA49 were diluted to an optical density (OD) of 0.1 at 600 nm (OD_{600} = 0.1; Hitachi Spectrophotometer U-5100). Test wafers were placed in a 10 mL snap-cap glass vial each and filled with 2.5 mL of fresh LB media and 0.5 mL of the diluted bacterial overnight culture. Test vials were tightly closed and horizontally placed on a rocker shaker (30 rpm/min) and incubated for 24 h at 37 °C.

Staining Procedure. Before staining the bacterial biofilms, the wafers were washed by a careful shaking step in a cell wash buffer (5 mM magnesium acetate; 10 mM TRIS-base; pH 8.0) and subsequently placed on a glass slide horizontally. The remaining biofilm on the wafer surfaces was stained at room temperature by carefully covering the surfaces with 200−300

μL of a mixed live/dead staining solution (Live/Dead BacLight Bacterial Viability Kit, ThermoFischer Scientific; 0.75 μL of Syto 9, 1.5 μL of propidium iodide/1 mL of cell wash buffer) for 15 min under humid conditions in the dark. After removing the supernatant staining solution, the wafers were washed again by a shaking step in a fresh cell wash buffer.

Microscope Analysis. After the final washing step, the wafers were prepared for microscope analysis immediately by placing 2−4 μL of BacLight mounting oil (ThermoFisher Scientific) onto the surfaces and covering the surfaces with round-shaped coverslips (0.9 cm in diameter). Epi-fluorescence microscopy was performed on an upright microscope (Axio-Imager M2, Zeiss, Germany) equipped with a light-emitting diode (LED) light source (Colibri 7, Zeiss, Germany) and a 630-fold magnification.

For imaging Syto 9 stained living bacteria, the Zeiss Colibri LED module 567 nm was used (50.30% light source intensity and an exposure time of 1.0 s) in combination with the corresponding filter cube system (Zeiss 15, BP 546/12; FT; 580; LP 590). An analysis of propidium iodide stained dead bacteria was performed using a Zeiss Colibri LED module 547 nm (4.27% light source intensity and 72.96 ms exposure time) with the corresponding filter cube system (Zeiss 10, BP 450−490; FT 510; BP 515−565).

The biofilm coverage rate [% covered area] was calculated by an interactive data analysis step using the Zeiss ZEN blue 3.2 software. The covered area data [μm^2] of each Syto 9 and propidium iodide images were put in relation to the total image size of 31.556 μm^2 (630× magnification).

Radial Distribution Function (RDF). To determine the spatial coverage of the bacterial colonies and their subsequent cluster formations after Cu incorporation, a radial distribution function (RDF) was implemented. The radial distribution function is summarized in

$$g_{PA}(r) = \frac{\langle \rho_{PA}(r) \rangle}{\rho} \tag{1}$$

Here, ρ_{PA} is the local density approximation of the bacteria (*P. aeruginosa*) and ρ is the bulk density. The local density is calculated using eq 2, where N^{inside} is the number of bacteria inside the ring. The area of the ring is $2\pi r\,dr$, where r is the radius of the inner circle and dr is the differential radius of the outer and inner circles.

$$\rho_{PA}(r) = \frac{N_{PA}^{inside}}{2\pi r\ dr} \tag{2}$$

The bulk density of the entire radial vicinity is calculated using eq 3, by dividing the total number of bacteria (N^{total}) by the area of the outer circle.

$$\rho = \frac{N_{PA}^{total}}{\pi(r + dr)^2} \tag{3}$$

RESULTS AND DISCUSSION

The synthesis of CSH phases on silicon wafers follows two steps. In the beginning, the native oxide layer on the silicon wafer was etched together with some silicon of the wafer. Afterward, the products of this etching reacted with the calcium hydroxide to form CSH phases. The synthesis of reproducible samples is dominated by many parameters, mainly concentration, temperature, pressure, size of the reactor, time, among others. We start our investigations with a comparison of the structure scanned in the electron microscope. It has been shown that it is possible to synthesize ultrathin (i.e., nanometer thick) calcium silicate hydrate (CSH) and calcium silicate (CS) phases on silicon wafers.[20,21,23−25] We will keep examining a comparison of parameters before and after the copper exchange. This is to investigate whether the incorporation of copper into the CSH substrates is successful, whether it leads to a change in the structure of the substrates, and how the copper interacts with the substrate.

SEM captions of representative samples, before and after the impregnation with Cu, are shown in Figure 1. Images A and C represent a sample without any copper incorporation, while images B and D represent a sample after the copper incorporation. The most important information one should take from these images is (1) that the structure of CSH phases has been synthesized successfully (as it can be compared to older literature) and (2) that the copper incorporation does not seem to manipulate this general structure. Fracturing the sample over a clean steel edge in an N_2-purged glovebox made local cross sections available. We have estimated the thickness of the CSH films (with copper incorporation) to be 180 nm.

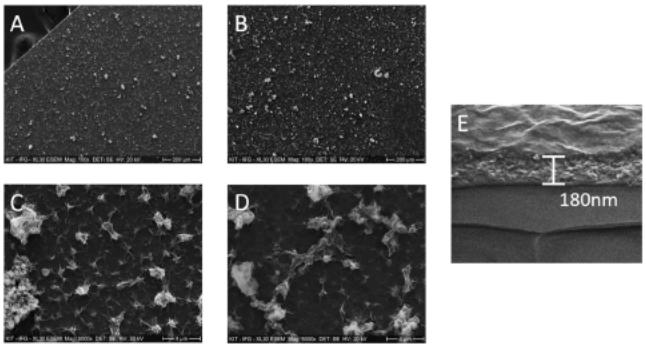

Figure 1. SEM gives an overview of the film's uniformity on a micrometer scale. Images (A, C) represent a sample without any copper incorporation, while images (B, D) represent a sample after copper incorporation. A fracture edge (E) makes a local cross section available.

While the SEM can give much information about the structure of the substrate, there is no information about chemical interactions. For this reason, we consider next the FT-IR, measured for the same sample in between all synthesis steps. This ensures accurate referencing. Figure 2 depicts the spectra of the synthesized CSH phases referenced to the piranha-cleaned silicon wafer (blue lines). The synthesis shows vibrational modes associated with the presence of not only silicates but also carbonates that are identified via their deformation modes ($\delta(CO_3^{2-})$ with a maximum at 873 cm^{-1}). Another two features relate to the presence of OH: a broad band between 3100 and 3500 cm^{-1} corresponding to bulk water and sharp peaks at 3690 and 3740 cm^{-1} that confirm the presence of dissociated water as Ca−OH and Si−OH, respectively. The spectra show vibrational modes corresponding to Si−O as well (ν(Si−O) centered at 1012 cm^{-1} and δ(Si−O−Si) below 750 cm^{-1}). These Si−O vibrations together with the presence of CaO−H and SiO−H provide evidence of the formation of CSH phases. Possible Cu−O vibrational modes can be found at 603 and 497 cm^{-1} (Cu^{2+}).

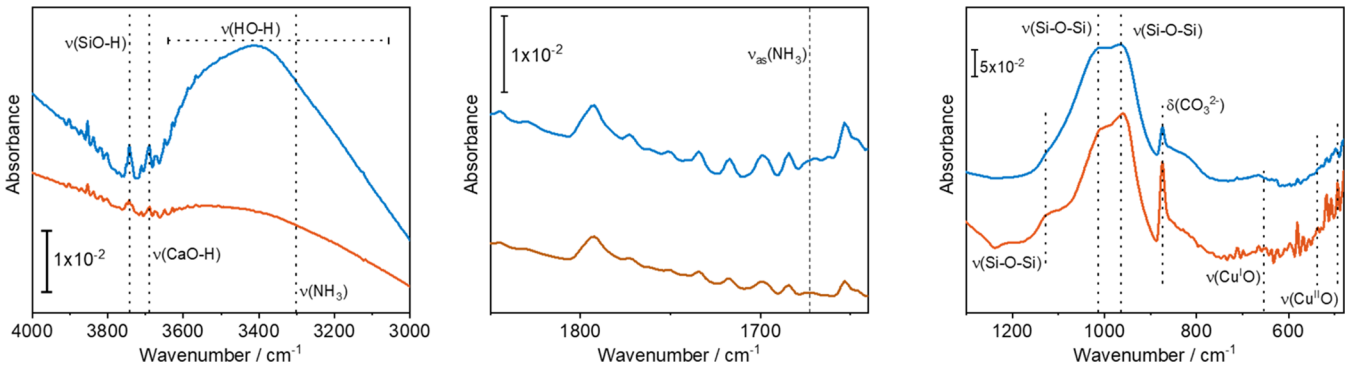

Figure 2. FT-IR absorption spectra token before (blue line) and after (red line) the incorporation of Cu into the CSH samples, referenced to the initial piranha-cleaned surface.

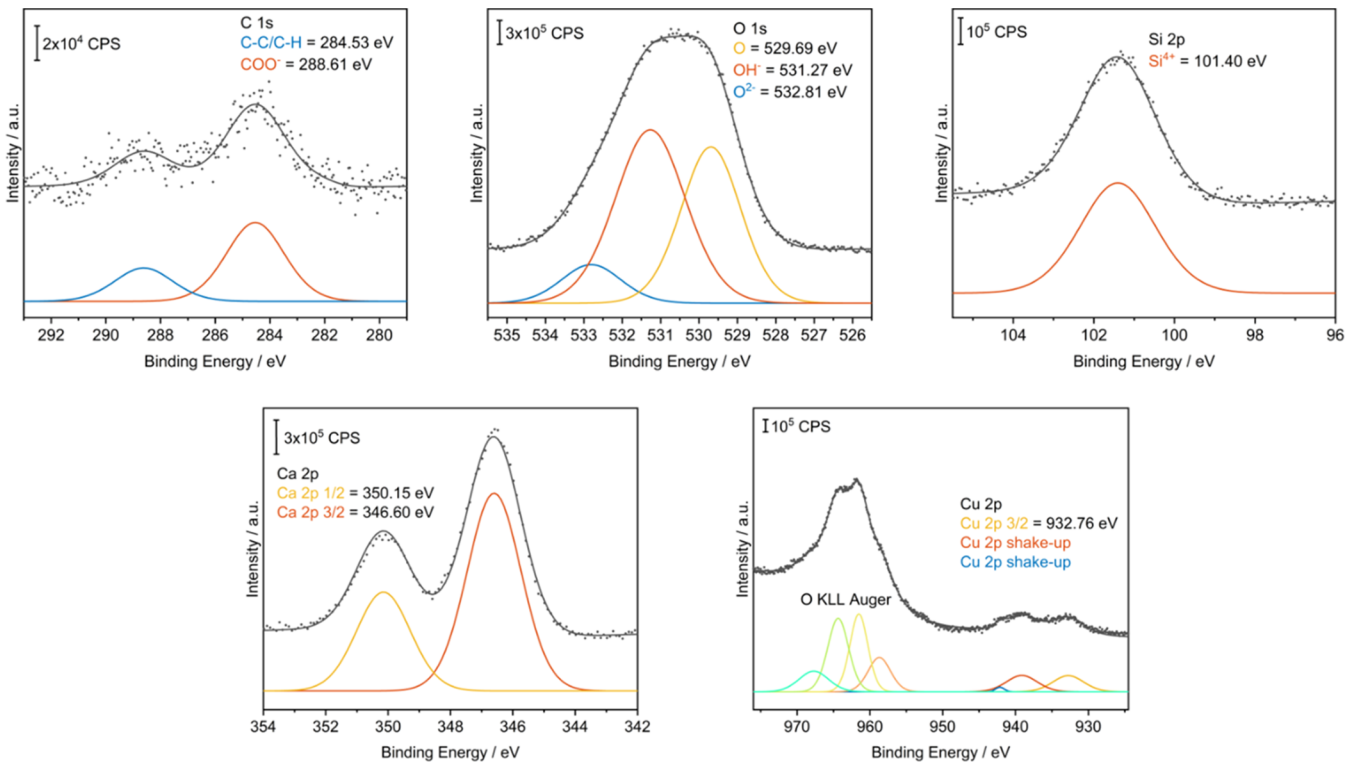

Figure 3. Core XP spectra of the surface after the incorporation of Cu into the CSH samples.

Other vibrational modes of Cu^{1+} have been reported by Baia et al. in the spectral range of 660 cm^{-1}.[26]

Cu−CSH samples were immersed in an aqueous solution of $[Cu(NH_3)_4](OH)_2$. No signal of gaseous ammonia is evident in the FT-IR measurement after the ion exchange. Possible infrared peaks might be found at 3300 cm^{-1} (symmetric NH_3 stretching mode), 1660 cm^{-1} (asymmetric stretching mode), and 1100 cm^{-1} (umbrella mode). Similarly, no modes of dissolved ammonia (NH_4^+ ion with tetrahedral symmetry) could be identified. This guides us to the conclusion that the incorporation of the copper ion was accompanied by ligand exchange. We suspect the CSH-backbone structure to be the new ligand, with the mechanism equivalent to other exchange reactions.[35]

While the IR absorbance spectra provide evidence for the chemisorption of copper in the CSH substrate, it is difficult to know if the copper remains oxidized because different vibrational modes occur in the 400−700 cm^{-1} region, overlapping the associated Cu−O vibrational modes. Therefore, complementary X-ray photoelectron spectroscopy (XPS) measurements were performed.

XPS provides information about the chemical composition of the substrate (Figure 3). Three contributions, the O^{2-} of the oxide, the OH^- of the hydroxide, and the contributions of adsorbed/incorporated water and oxygen as part of the adsorbed carboxylic acid groups, appear in the range of 529−533 eV. The contribution of oxygen-containing organic species is in the range of 1 atom% and, for this reason, can be neglected in these studies. The Ca/Si ratio was determined to be 0.78 from the XPS areas of CaO and SiO_2. The mean Ca/Si ratio of CSH phases in commercial cement differs significantly, from 0.7 to 2.3.[27]

The Cu 2p region has two prominent peaks around 953 and 933eV, characteristic of Cu $2p_{1/2}$ and Cu $2p_{3/2}$ peaks, respectively. The smaller peaks around 943 and 940 eV are characteristic satellite features found only in samples with Cu^{2+}

species. The biggest challenge in using XPS to study samples with different copper species of mixed oxidation states is the substantial overlap of the Cu 2p peaks for Cu^{2+} and reduced species such as Cu^{1+} and metallic Cu^{0}. A method to fit individual peaks exactly into the XP spectra has been reported by Biesinger et al.[28] They examined several pure $Cu(OH)_2$ and CuO samples with XPS to determine the ratios of the Cu^{2+} peaks to shake-up peak areas. It has been shown that the areas of the Cu^{2+} peaks are a certain multiple of the combined shake-up peak areas. However, these values depend on the electronic structure of the Cu species. They determined the ratios of 1.57 ± 0.1 for pure $Cu(OH)_2$ and 1.89 ± 0.08 for pure CuO samples. These results enabled reliable analysis of the complex Cu 2p spectra for samples with mixed oxidation states of copper.

XPS shows the composition of the outer 5−10 nm of the sample (Table 1). For our investigations, we want to reach a

Table 1. XPS Measurements of the Atomic Composition after the Incorporation of Cu into the CSH Samples

substrate	element, orbital	position/ eV	species	area	atom %
Cu−CSH	C, 1s	284.53	C−C/ C−H	31119.98	5.4
		288.61	COOR	13180.08	
	O, 1s	529.69	metal-oxide	98041.05	64.2
		531.27	OH	397016.74	
		532.81	silicate	516957.26	
	Si, 2p	101.40	silicate	102655.51	16.8
	Ca, $2p_{3/2}$	346.60	CSH	387866.95	12.9
	Ca, $2p_{1/2}$	350.15	CSH	193933.48	
	Cu, $2p_{3/2}$	932.76	Cu_2O/ CuO	5929.6	0.7

quasi-3D description of the distribution of the elements inside the copper-coated samples. Thus, in the next step, we consider the investigations of our samples by ToF-SIMS. First, the lateral distribution of the most important components was measured. Afterward, certain masses were monitored under constant sputter conditions. The results of these measurements are shown in Figure 4.

To understand the interactions of our prepared Cu−CSH samples with the environment, namely, bacteria, it is important to investigate how much copper is immobilized inside the structure of the samples. Our Cu−CSH samples were stored in 10 mL of water for different times at room temperature to determine the degree of leaching (Table 2).

The Cu/Ca ratio of ICP-OES (etched sample) is 0.03. This is nearly 2 times lower than the concentration investigated by XPS measurements. These two types of measurements are difficult to compare, as the XPS represents a surface scanning method with a low depth of information (5−10 nm), while the ICP-OES data represents the copper concentration of the whole sample.

The biofilm formation was studied using a *P. aeruginosa* strain, PA49, which was previously isolated from contaminated natural water samples and characterized. As commonly accepted *P. aeruginosa*, a Gram-negative rod-shaped bacterium, is a good biofilm former. Control CSH silicon waver slides and CSH Cu(II)-coated surfaces were incubated in an overnight culture of PA49 using an LB high nutrient broth for intensive biofilm formation. After microscopy preparation for living/dead imaging, the surfaces were analyzed for biofilm coverage rate and survival capacities after 24 h of incubation in a bacterial suspension.

A powerful way to investigate the images is the radial distribution function (RDF): while the copper-free CSH phase shows a completely random distribution of *P. aeruginosa* bacteria in biofilms (Figure 5, bottom), the samples with copper incorporation (Cu−CSH) (Figure 5, bottom) reveal also the bacterial colonization of the modified surfaces but with an enhanced cluster formation on the surfaces. In addition to these morphological distinctive features, these images demonstrated initially the invalidity of the newly modified Cu−CSH-coated surfaces concerning its differences in biofilm formation. This became also visible when comparing the dead or injured percentage stained with propidium iodide (PI). Most of the bacteria were alive when colonizing both kinds of surfaces (CSH and Cu−CSH).

The statistical evaluation of the defined coverage of surface area was quantified from both bacterial cell fluorescence signals: the green fluorescent living cells and the red fluorescent dead or injured cells. It became obvious in Table 3 that surfaces coated with Cu−CSH were less densely covered with only calculated 44.4% in comparison to CSH-modified surfaces. The mean percentage of coverage mentioning living and dead bacteria was found to be 17.64% in the case of CSH-modified surfaces. In contrast, only 7.84% of the measured areas of the Cu−CSH-modified surfaces were covered with attached bacterial cells. The propidium iodide stained dead or injured bacteria was presented as the percentage of the total covered area size for both different modified surfaces. In the case of CSH surface, this was calculated to be about 1.8% and in the case of Cu−CSH, it was 1.7%. In fact, the percentage of dead or injured cells coverage did not differ significantly in contrast to the coverage percentage of the living cells.

Different reasons and interpretations must be discussed for the optimization of these first results. (i) Bacteriotoxic Cu concentrations were found to be in the range of 1.5 μg/L in water.[29] Hence, immobilized Cu(II) concentrations of the Cu−CSH coatings are suspected not to reach bactericidal metal concentrations. Different analyses demonstrated a nonleaching of copper (in contrast to Ca) even after 24 h, as mentioned in Table 2. (ii) The impact of immobilized Cu(II) on procaryotic cells is less efficient compared to that of bulk Cu ions. Here, the exact biocidal mechanisms of copper on *P. aeruginosa* PA49 need to be known as well susceptibility of *P. aeruginosa* for copper is important. The *P. aeruginosa* PA49 strain was studied previously for its antibiotic resistance profile and was found to be resistant to up to seven different clinically relevant antibiotic drugs.[30] It has to be analyzed if the antibiotic resistances also possess a cross-resistance against the impacts of heavy metals.[29]

In addition to the biofilm formation on the coated surfaces using the DNA fluorescence dye Syto 9, which binds to DNA in general (green fluorescence), dead or injured bacteria in biofilms are stained with propidium iodide (red fluorescence) due to the nonintact membrane potential of the cells and binding to the DNA afterward. In Figure 5 and Table 3, it became obvious that only a small part of the stained biofilm consisted of dead or injured cells (1−2%). The dominating part of the biofilms consisted of living *P. aeruginosa* bacteria. All results underline the partly apparent validity of the Cu−CSH coatings under the applied parameters compared to coatings without copper.

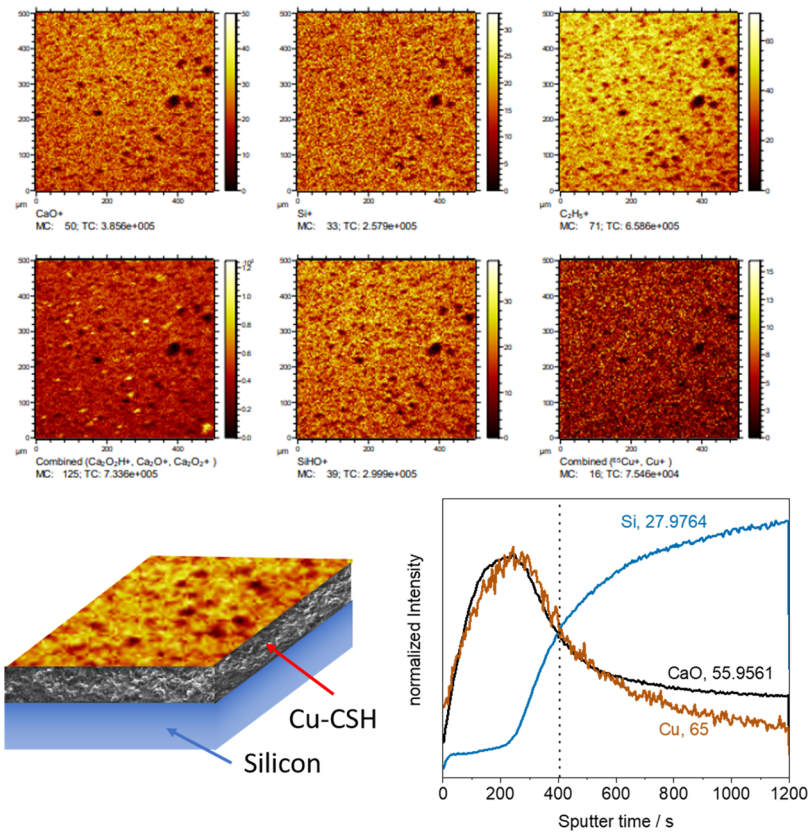

Figure 4. Lateral distribution of all components is very homogeneous, and this applies to all samples. The copper signal is correlated with CaO of the respective samples along the sputtering time. This points to the incorporation of copper into the CSH volume.

Table 2. Results from Cu−CSH Samples Stored in 10 mL of Water for Different Times at Room Temperature to Determine the Degree of Leaching

name of the sample	element	concentration in mg/L
Cu-exchanged, leached for 1 h	Ca	1.14
	Cu	<0.007
Cu-exchanged, leached for 3 h	Ca	1.09
	Cu	<0.007
Cu-exchanged, leached for 6 h	Ca	1.67
	Cu	<0.007
Cu-exchanged, leached for 17 h	Ca	1.16
	Cu	<0.007
Cu-exchanged, leached for 24 h	Ca	1.76
	Cu	<0.007
Cu-exchanged, 1 h etched by HCl	Ca	0.474
	Cu	0.016

Many studies underlined that bacteria are killed by copper ions released from surfaces. This process seems to be more effective in killing bacteria but bears the risk of unwanted interactions with evolutionary higher organisms in concern of cytotoxicities on cells. From the microbiological point of view, copper ions enter the bacterial cells and interact with different protein clusters, resulting in modified and enhanced ROS (reactive oxygen species), which are responsible for bacteria injuries or death.[31] In contrast, copper-incorporated surfaces without any metal leaching are favored in this study to avoid unwanted side reactions induced by the released copper ions. However, it has to be studied whether the contact of the bacteria with copper-incorporated surfaces is also an important and valid structure for killing bacteria. Previous studies with *Enterococcus hirae* demonstrated that the concentration of copper ions released from modified surfaces was not high enough to impact this Gram-positive bacterium.[32] Hence, an alternative impact of solid metal or immobilized copper on bacteria survival has to be discussed.

In fact, it was demonstrated that bacteria in contact with dry Cu surfaces, in contrast to bulk exposed Cu ions, do not proliferate and most of them are killed within minutes.[31] Recent studies suggest that cells are not killed via the accumulation of lethal mutations but rather due to the initial damage of membranes.[33−36] This, in turn, also leads to DNA damage and the killing of cells. In consequence, this gives the impression of genotoxicity as the underlying mechanism of killing. Conversely, it is more likely that lipid peroxidation or irreversible inactivation of essential membrane proteins compromises membranes of exposed cells of Cu surface beyond the point of recovery.[31]

Our approach opens up new perspectives addressing the transport properties of the rim zone, which is essential for chemical resilience in aggressive environments. Furthermore, performance-oriented tailoring of the surface chemistry of the compounds of porous systems represents an interesting challenge to improve the durability without impairing the strength as well as the temperature resistance of the material and counteracting in this way the potential shortcomings of conventional surface protection systems. We believe that the detailed knowledge from basic research can finally be transferred to industry for innovation. The incorporation of new metals would be possible at different points during the production of porous materials.

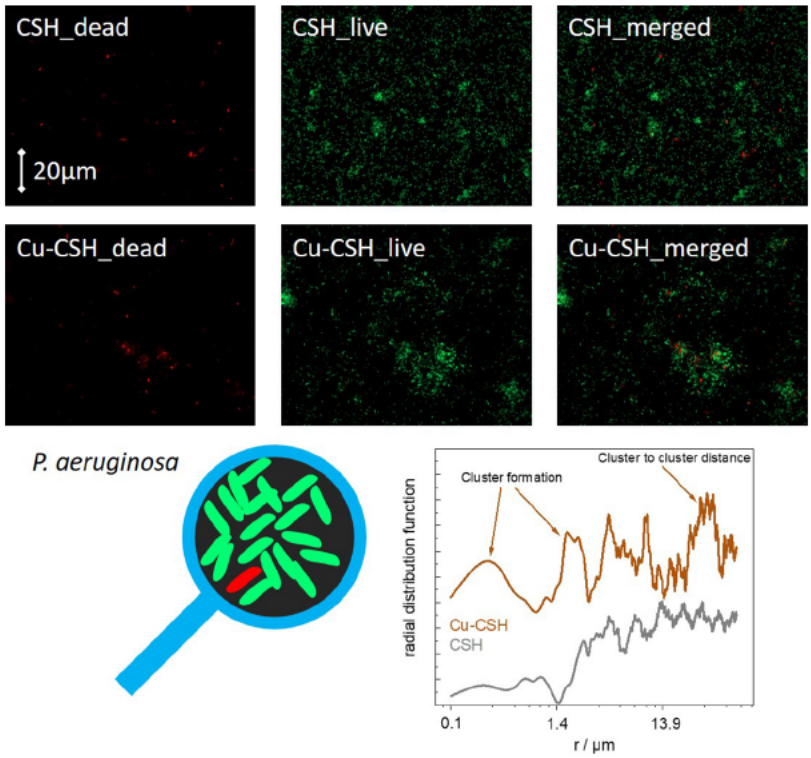

Figure 5. Two exemplary images of CSH (upper line) and Cu−CSH-coated Si-wafer surfaces (middle line): Living bacteria appear green fluorescent by Syto 9 and dead/damaged bacteria appear red fluorescent by the propidium iodide staining procedure. In the bottom line, one can see the radial distribution function (RDF) determined from several images: While the gray line of the PA49 (on CSH) generates a random distribution, certain peaks are found in the RDF of the PA49 on Cu−CSH. Due to the rod shape of the PA, two different distances can be seen in the cluster formation; one below 1 μm and one around 2 μm. The other peaks appearing in this distribution point to cluster-to-cluster distance.

Table 3. Biofilm Coverage Rate [%]: Coverage Rates on CSH and Cu−CSH Surfaces Grown Bacterial Biofilms Were Calculated in Relation to the Total Image Size[a]

bacterial covered area as a percentage to total image size [%]		image 1	image 2	image 3	image 4	mean	SD	coverage of live or dead bacteria as a percentage to total covered area [%]
CSH	live	10.7	14.5	19.9	24.3	17.33	6.0	98.2
	dead	0.4	0.2	0.2	0.4	0.31	0.1	1.8
Cu−CSH	live	4.2	7.2	6.7	12.6	7.70	3.5	98.3
	dead	0.1	0.1	0.1	0.2	0.13	0.1	1.7

[a]Statistical calculation was done by coverage data of four different images randomly taken from the sample surfaces.

CONCLUSIONS

The formation of biofilms is a problem today in general and is accompanied by material degradation. For calcium silicate hydrate (CSH) phases, we have investigated a possible chemical modification to incorporate copper by the so-called metal−metal exchange reaction (MMER). This modification of CSH with copper from solutions of $[Cu(NH_3)_4](OH)_2$ yields surfaces already with low total copper concentrations. The distribution of the copper inside the CSH films was very homogeneous, laterally and in-depth. In contrast to calcium, no leaching was found for the copper in contact with liquids. As was expected for this work, the prepared samples seem to have a bio-repellent character. This was underlined by fluorescence microscopy of the samples on which biofilms were applied from dispersions of *P. aeruginosa*. While the copper-free CSH phase shows a completely random distribution of the bacteria in biofilms, the samples with copper incorporation reveal lower bacterial colonization of the modified surfaces with an enhanced cluster formation.

AUTHOR INFORMATION

Corresponding Author

Peter Thissen − *Institut für Funktionelle Grenzflächen (IFG), Karlsruher Institut für Technologie (KIT), 76344 Eggenstein-Leopoldshafen, Deutschland; Institut für Massivbau und Baustofftechnologie (IMB), Karlsruher Institut für Technologie (KIT), 76131 Karlsruhe, Deutschland;* orcid.org/0000-0001-7072-4109; Email: peter.thissen@kit.edu

Authors

Thomas Schwartz − *Institut für Funktionelle Grenzflächen (IFG), Karlsruher Institut für Technologie (KIT), 76344 Eggenstein-Leopoldshafen, Deutschland*

Nils Schewe − *Institut für Funktionelle Grenzflächen (IFG), Karlsruher Institut für Technologie (KIT), 76344 Eggenstein-Leopoldshafen, Deutschland;* orcid.org/0000-0001-6283-4834

Matthias Schwotzer − *Institut für Funktionelle Grenzflächen (IFG), Karlsruher Institut für Technologie (KIT), 76344 Eggenstein-Leopoldshafen, Deutschland*
Marita Heinle − *Institut für Funktionelle Grenzflächen (IFG), Karlsruher Institut für Technologie (KIT), 76344 Eggenstein-Leopoldshafen, Deutschland*
Ammar Mahmood − *Institut für Massivbau und Baustofftechnologie (IMB), Karlsruher Institut für Technologie (KIT), 76131 Karlsruhe, Deutschland*
Peter Krolla − *Institut für Funktionelle Grenzflächen (IFG), Karlsruher Institut für Technologie (KIT), 76344 Eggenstein-Leopoldshafen, Deutschland*

Author Contributions

§ T.S. and N.S. contributed equally to this paper.

Notes

The authors declare no competing financial interest.

ACKNOWLEDGMENTS

The results presented in this article have been obtained within DFG-funded project TH 1566/6-1.

REFERENCES

(1) Pan, S.; Richardson, J. J.; Christofferson, A. J.; Besford, Q. A.; Zheng, T.; Wood, B. J.; Duan, X.; Jara Fornerod, M. J.; McConville, C. F.; Yarovsky, I.; Guldin, S.; Jiang, L.; Caruso, F. Fluorinated Metal−Organic Coatings with Selective Wettability. *J. Am. Chem. Soc.* **2021**, *143*, 9972−9981.
(2) Taylor, S. R.22-The Role of Intrinsic Defects in the Protective Behavior of Organic Coatings. In *Handbook of Environmental Degradation of Materials*, 2nd ed.; Kutz, M., Ed.; William Andrew Publishing: Oxford, 2012; pp 655−672.
(3) Mitra, D.; Kang, E.-T.; Neoh, K. G. Antimicrobial Copper-Based Materials and Coatings: Potential Multifaceted Biomedical Applications. *ACS Appl. Mater. Interfaces* **2020**, *12*, 21159−21182.
(4) Ryan, E. J.; Ryan, A. J.; González-Vázquez, A.; Philippart, A.; Ciraldo, F. E.; Hobbs, C.; Nicolosi, V.; Boccaccini, A. R.; Kearney, C. J.; O'Brien, F. J. Collagen scaffolds functionalised with copper-eluting bioactive glass reduce infection and enhance osteogenesis and angiogenesis both in vitro and in vivo. *Biomaterials* **2019**, *197*, 405−416.
(5) Gross, T. M.; Lahiri, J.; Golas, A.; Luo, J.; Verrier, F.; Kurzejewski, J. L.; Baker, D. E.; Wang, J.; Novak, P. F.; Snyder, M. J. Copper-containing glass ceramic with high antimicrobial efficacy. *Nat. Commun.* **2019**, *10*, No. 1979.
(6) Wu, K.; Douglas, S. P.; Wu, G.; MacRobert, A. J.; Allan, E.; Knapp, C. E.; Parkin, I. P. A rugged, self-sterilizing antimicrobial copper coating on ultra-high molecular weight polyethylene: a preliminary study on the feasibility of an antimicrobial prosthetic joint material. *J. Mater. Chem. B* **2019**, *7*, 3310−3318.
(7) Kredl, J.; Kolb, J. F.; Schnabel, U.; Polak, M.; Weltmann, K.-D.; Fricke, K. Deposition of Antimicrobial Copper-Rich Coatings on Polymers by Atmospheric Pressure Jet Plasmas. *Materials* **2016**, *9*, No. 274.
(8) Li, M.; Gao, L.; Schlaich, C.; Zhang, J.; Donskyi, I. S.; Yu, G.; Li, W.; Tu, Z.; Rolff, J.; Schwerdtle, T.; Haag, R.; Ma, N. Construction of Functional Coatings with Durable and Broad-Spectrum Antibacterial Potential Based on Mussel-Inspired Dendritic Polyglycerol and in Situ-Formed Copper Nanoparticles. *ACS Appl. Mater. Interfaces* **2017**, *9*, 35411−35418.
(9) Gosau, M.; Bürgers, R.; Vollkommer, T.; Holzmann, T.; Prantl, L. Effectiveness of antibacterial copper additives in silicone implants. *J. Biomater. Appl.* **2013**, *28*, 187−198.
(10) Mitra, D.; Li, M.; Kang, E.-T.; Neoh, K. G. Transparent Copper-Loaded Chitosan/Silica Antibacterial Coatings with Long-Term Efficacy. *ACS Appl. Mater. Interfaces* **2017**, *9*, 29515−29525.
(11) Flemming, H.-C.; Neu, T. R.; Wozniak, D. J. The EPS matrix: the "house of biofilm cells". *J. Bacteriol.* **2007**, *189*, 7945−7947.
(12) Bixler, G. D.; Bhushan, B. Biofouling: lessons from nature. *Philos. Trans. R. Soc., A* **2012**, *370*, 2381−2417.
(13) Costerton, J. W.; Stewart, P. S.; Greenberg, E. P. Bacterial Biofilms: A Common Cause of Persistent Infections. *Science* **1999**, *284*, 1318−1322.
(14) Stewart, P. S.; Franklin, M. J. Physiological heterogeneity in biofilms. *Nat. Rev. Microbiol.* **2008**, *6*, 199−210.
(15) Flemming, H.-C.; Wingender, J. The biofilm matrix. *Nat. Rev. Microbiol.* **2010**, *8*, 623−633.
(16) Wimpenny, J.; Manz, W.; Szewzyk, U. Heterogeneity in biofilms. *FEMS Microbiol. Rev.* **2000**, *24*, 661−671.
(17) Glinel, K.; Thebault, P.; Humblot, V.; Pradier, C. M.; Jouenne, T. Antibacterial surfaces developed from bio-inspired approaches. *Acta Biomater.* **2012**, *8*, 1670−1684.
(18) Allen, A. J.; Thomas, J. J.; Jennings, H. M. Composition and density of nanoscale calcium−silicate−hydrate in cement. *Nat. Mater.* **2007**, *6*, 311−316.
(19) Makul, N.; Fediuk, R.; Szelag, M. Advanced interactions of cement-based materials with microorganisms: A review and future perspective. *J. Build. Eng.* **2022**, *45*, No. 103458.
(20) Giraudo, N.; Wohlgemuth, J.; Bergdolt, S.; Heinle, M.; Thissen, P. Passivation of Hydrated Cement. *ACS Sustainable Chem. Eng.* **2018**, *6*, 727−737.
(21) Burek, K.; Krause, F.; Schwotzer, M.; Nefedov, A.; Süssmuth, J.; Haubitz, T.; Kumke, M. U.; Thissen, P. Hydrophobic Properties of Calcium-Silicate Hydrates Doped with Rare-Earth Elements. *ACS Sustainable Chem. Eng.* **2018**, *6*, 14669−14678.
(22) Thissen, P.; Peixoto, T.; Longo, R. C.; Peng, W.; Schmidt, W. G.; Cho, K.; Chabal, Y. J. Activation of Surface Hydroxyl Groups by Modification of H-Terminated Si(111) Surfaces. *J. Am. Chem. Soc.* **2012**, *134*, 8869−8874.
(23) Giraudo, N.; Bergdolt, S.; Laye, F.; Krolla, P.; Lahann, J.; Thissen, P. Dehydration and dehydroxylation of C-S-H phases synthesized on silicon wafers. *Appl. Surf. Sci.* **2018**, *433*, 589−595.
(24) Longo, R. C.; Königer, F.; Nefedov, A.; Thissen, P. Chemical Properties of Metal-Silicates Rendered by Metal Exchange Reaction. *ACS Sustainable Chem. Eng.* **2019**, *7*, 8449−8457.
(25) Longo, R. C.; Schewe, N.; Weidler, P. G.; Heissler, S.; Thissen, P. Synthesis of Silicates for High-Performance Oxide Semiconductors: Electronic Structure Analysis. *ACS Appl. Electron. Mater.* **2021**, *3*, 299−308.
(26) Popescu, R. A.; Magyari, K.; Vulpoi, A.; Trandafir, D. L.; Licarete, E.; Todea, M.; Ştefan, R.; Voica, C.; Vodnar, D. C.; Simon, S.; Papuc, I.; Baia, L. Bioactive and biocompatible copper containing glass-ceramics with remarkable antibacterial properties and high cell viability designed for future in vivo trials. *Biomater. Sci.* **2016**, *4*, 1252−1265.
(27) Ebbert, C.; Grundmeier, G.; Buitkamp, N.; Kröger, A.; Messerschmidt, F.; Thissen, P. Toward a microscopic understanding of the calcium−silicate−hydrates/water interface. *Appl. Surf. Sci.* **2014**, *290*, 207−214.
(28) Biesinger, M. C. Advanced analysis of copper X-ray photoelectron spectra. *Surf. Interface Anal.* **2017**, *49*, 1325−1334.
(29) Seiler, C.; Berendonk, T. U. Heavy metal driven co-selection of antibiotic resistance in soil and water bodies impacted by agriculture and aquaculture. *Front. Microbiol.* **2012**, *3*, No. 399.
(30) Berditsch, M.; Jäger, T.; Strempel, N.; Schwartz, T.; Overhage, J.; Ulrich, A. S. Synergistic Effect of Membrane-Active Peptides Polymyxin B and Gramicidin S on Multidrug-Resistant Strains and Biofilms of *Pseudomonas aeruginosa*. *Antimicrob. Agents Chemother.* **2015**, *59*, 5288−5296.
(31) Dupont, C. L.; Grass, G.; Rensing, C. Copper toxicity and the origin of bacterial resistance–new insights and applications. *Metallomics* **2011**, *3*, 1109−1118.

(32) Mathews, S.; Hans, M.; Mücklich, F.; Solioz, M. Contact killing of bacteria on copper is suppressed if bacterial-metal contact is prevented and is induced on iron by copper ions. *Appl. Environ. Microbiol.* **2013**, *79*, 2605−2611.
(33) Espírito Santo, C.; Morais, P. V.; Grass, G. Isolation and characterization of bacteria resistant to metallic copper surfaces. *Appl. Environ. Microbiol.* **2010**, *76*, 1341−1348.
(34) Espírito Santo, C.; Taudte, N.; Nies, D. H.; Grass, G. Contribution of copper ion resistance to survival of Escherichia coli on metallic copper surfaces. *Appl. Environ. Microbiol.* **2008**, *74*, 977−986.
(35) Espírito Santo, C.; Lam, E. W.; Elowsky, C. G.; Quaranta, D.; Domaille, D. W.; Chang, C. J.; Grass, G. Bacterial killing by dry metallic copper surfaces. *Appl. Environ. Microbiol.* **2011**, *77*, 794−802.
(36) Quaranta, D.; Krans, T.; Espírito Santo, C.; Elowsky, C. G.; Domaille, D. W.; Chang, C. J.; Grass, G. Mechanisms of contact-mediated killing of yeast cells on dry metallic copper surfaces. *Appl. Environ. Microbiol.* **2011**, *77*, 416−426.